Research

Unlocking Cancer Glycomes from Histopathological Formalin-fixed and Paraffin-embedded (FFPE) Tissue Microdissections*[S]

Hannes Hinneburg‡§, Petra Korać¶, Falko Schirmeister‡§, Slavko Gasparov‖**, Peter H. Seeberger‡§, Vlatka Zoldoš¶, and Daniel Kolarich‡ ‡§§

N*- and *O*-glycans are attractive clinical biomarkers as glycosylation changes in response to diseases. The limited availability of defined clinical specimens impedes glyco-biomarker identification and validation in large patient cohorts. Formalin-fixed paraffin-embedded (FFPE) clinical specimens are the common form of sample preservation in clinical pathology, but qualitative and quantitative *N*- and *O*-glycomics of such samples has not been feasible to date. Here, we report a highly sensitive and glycan isomer selective method for simultaneous *N*- and *O*-glycomics from histopathological slides. As few as 2000 cells isolated from FFPE tissue sections by laser capture microdissection were sufficient for in-depth histopathology-glycomics using porous graphitized carbon nanoLC ESI-MS/MS. *N*- and *O*-glycan profiles were similar between unstained and hematoxylin and eosin stained FFPE samples but differed slightly compared with fresh tissue. This method provides the key to unlock glyco-biomarker information from FFPE histopathological tissues archived in pathology laboratories worldwide. *Molecular & Cellular Proteomics 16: 10.1074/mcp.M116.062414, 524–536, 2017.

Cell surface and body fluid proteins are extensively decorated with specific glycans (1). Glycoproteins and glycolipids are part of the plasma membrane glycocalyx, the first interface for intercellular interactions (2). As such, the glycome and glycoproteome are key elements of cellular communication (3, 4). In many disease states, biological processes change to express different glycans and glycoproteins on the cell surface (5, 6). Dynamic changes of the glycome are a result of age, an organism's physiological state (homeostasis or disease) and various other environmental or intrinsic factors (7–9). As glycans integrate environmental and indirectly genetic factors and are closely associated with complex diseases, they have been established as predictive and prognostic markers for diseases such as cancer and chronic inflammation (6, 10–13).

Most efforts to identify glyco-biomarkers focused on body fluids because of the ease of accessibility (6, 14, 15). To better understand the molecular events responsible for disease onset and progression, analysis of specific glycosylation signatures directly from tissue specimens is fundamental (16–18). However, tissues are often highly heterogeneous mixtures of different cell types that hamper the detection of specific markers. The collection of significant numbers of well-defined clinical tissue specimens for high quality biomarker research is challenging because of ethical and technical obstacles.

A widely applied standard pathology procedure is the preservation of tissue samples by formalin fixation followed by subsequent paraffin-embedding (FFPE)[1], along with *e.g.* hematoxylin and eosin (H&E) staining (19) for tumor diagnosis and long-term conservation. Many FFPE preserved tissue specimens are available in clinical centers around the world and are often associated with comprehensive clinical data sets. FFPE tissues can be handled at ambient temperatures and various dissection methods such as laser capture microdissection can be applied in order to minimize contaminations by other tissues and/or cells. This makes them a highly valuable source for any disease related research, biomarker discovery or retrospective studies, as long as the compounds

From the ‡Max Planck Institute of Colloids and Interfaces, Department of Biomolecular Systems, 14424 Potsdam, Germany; §Freie Universität Berlin, Department of Biology, Chemistry, Pharmacy, Institute of Chemistry and Biochemistry, 14195 Berlin, Germany; ¶Faculty of Science, Department of Biology, Division of Molecular Biology, University of Zagreb, Zagreb, Croatia; ‖Institute for Pathology and Cytology, University Hospital Merkur, Zagreb, Croatia; **Department of Pathology, Medical School Zagreb, University of Zagreb, Zagreb, Croatia

Received July 19, 2016, and in revised form, January 22, 2017
Published, MCP Papers in Press, January 25, 2017, DOI 10.1074/mcp.M116.062414
Author contributions: H.H. and D.K. designed research; H.H. and P.K. performed research; F.S. contributed new reagents or analytic tools; H.H. and F.S. analyzed data; H.H., P.K., F.S., P.H.S., V.Z., and D.K. wrote the paper; P.K. sample collection/preparation; S.G. collected and provided tissue samples.

[1] The abbreviations used are: FFPE, formalin-fixed and paraffin-embedded; AUC, area under the curve; BPC, base peak chromatogram; EIC, extracted ion chromatogram; H&E, hematoxylin and eosin; HCC, hepatocellular carcinoma; LC, liquid chromatography; LCM, laser capture microdissection; MS/MS, tandem mass spectrometry; PGC, porous graphitized carbon; SPS, smart parameter setting; ICC, ion charge control.

of interest are qualitatively and quantitatively preserved and can likewise be extracted for further analyses (20–22).

Proteins (20, 21, 23–25) or nucleic acids (23, 26, 27) are now frequently recovered from FFPE specimens even though they can be modified and/or degraded during the conservation process. The analysis of metabolites (28), glycosaminoglycans (29), as well as *N*- (25, 30–33) and *O*-glycans (32–34) has been described. To date, all analyses aimed at comprehensive clinical tissue *N*- and *O*-glycomics (1) suffered from poor sensitivity (32), (2) could not be applied to both *N*- and *O*-glycans (25, 30, 31, 34), (3) fall short of reliable *O*-glycan extraction (33), (4) suffered from the differentiation of isobaric *N*- and *O*-glycans (30, 32, 33) or reliable analysis of intact sialylated glycans (30, 31). Thus, a robust method for the sensitive and selective extraction and in-depth analysis of FFPE tissue derived *N*- and *O*-glycans is required.

Here we present a highly sensitive approach to individually and sequentially extract and analyze structurally preserved *N*- and *O*-glycans from as few as 1000 cells isolated from FFPE tissue specimens. Laser capture microdissection (LCM) ensures contact free picking-up of cell groups or even a single cell for easy subsequent manipulation. LCM isolated tissues were analyzed along with whole tissue sections using porous graphitized carbon (PGC) nano scale liquid chromatography (nanoLC) coupled with online ESI tandem mass spectrometric (MS/MS) detection (35, 36). In-depth glycan structure information on fucose and sialic acid linkages was obtained within a single experiment providing a maximum of information from a minimal amount of clinical material. This PGC nanoLC-ESI MS/MS based glycomics approach applied onto LCM-isolated cells derived from FFPE tissue specimens is opening novel avenues for investigating the role of protein glycosylation in health and disease.

EXPERIMENTAL PROCEDURES

If not otherwise stated all materials were purchased in the highest possible quality from Sigma-Aldrich (St. Louis, MO). Peptide-*N*-Glycosidase F (PNGase F) was obtained from Roche Diagnostics GmbH (Mannheim, Germany). Water was used after purification with a Milli Q-8 direct system (Merck KGaA, Darmstadt, Germany). Chloroform was from VWR international (Fontenay-sous-Bois, France). Human liver tissue was derived from three different patients suffering from liver cirrhosis or hepatocellular carcinoma obtaining a liver transplant according to the Milan criteria. This study was approved by the Ethics committee of "*Klinieka Bolnica Merkur*" For reporting the glycomics experiments the MIRAGE guidelines are followed (37).

Formalin Fixation and Paraffin Embedding—Liver tissue was divided into several parts and either immediately frozen at −80 °C or fixed with formalin (Formalin solution, neutral buffered, 10%, BioGnost, Zagreb, Croatia) and embedded in paraffin (Paraffin wax, Sakura, Alphen aan den Rijn, The Netherlands) following routine procedures. Briefly, tissue went through 10% formalin (24 h), 70% ethanol (2 × 1 h), 95% ethanol (2 × 1 h), absolute ethanol (2 × 1 h), xylene (2 × 1 h at 37 °C) and liquid paraffin (3 × 1 h at 60 °C). Paraffin tissue blocks were cut into 2–10 μm thick sections using a standard sliding manual microtome (Microm, Dreiech, Germany). 2–4 μm thick sections were mounted onto glass slides (Microscope slides, Vitrognost). H&E staining was done according to routine protocols (19). After deparaffinization with xylene, and rehydration through decreasing series of ethanol, slides were washed and hematoxylin was applied. After subsequent washes and eosin treatment slides were dehydrated with increasing ethanol series and briefly air-dried. The specimens were used within 3 months after initial preparation.

Laser Capture Microdissection—Laser capture microdissection was done as follows: stained sections mounted on membrane slides (MembraneSlide 1.0 PEN, Carl Zeiss Microscopy, Jena, Germany) were analyzed under the microscope which is part of a laser microdissection system (Palm Zeiss MicroBeam, Axiovert 200M with PALM RoboSoftware, Carl Zeiss Microscopy) and selected cells were counted, marked and cut using PALM RoboSoftware according to manufacturer's manual.

Laser pressure catapulting method was performed using the protocol described in the manufacturer's manual and isolated tissue parts were collected in adhesive caps of 500 μl collection tubes (Sample AdhesiveCap 500 opaque (D) PCR Tube, Carl Zeiss Microscopy).

Protein Extraction/Antigen Retrieval from FFPE Tissues—

Unmounted Sample Set—Protein extraction of around 50 unmounted FFPE tissue sections was done as described previously (21). Briefly, 2–10 μm thick FFPE sections were transferred into 1.5 ml sample tubes, washed twice in xylene for 5 min under mild agitation, followed by two washes with absolute ethanol for 5 min before being allowed to dry. Deparaffinized and washed samples were combined and homogenized on ice in a 0.1 M Tris-HCl, pH 8.0; 0.1 M DTT buffer using a table top Branson sonifier B-12 sonicator (Branson Sonic Power output control: 1.5; 3 × 10–30 s). SDS was added to a final concentration of 4% (w/v) and samples were incubated at 99 °C for 60 min under mild agitation and were allowed to cool down to room temperature afterward. Subsequently, the samples were centrifuged for 20 min at 2,000 rcf to remove nonsoluble material. Proteins were precipitated from supernatant according to the method used by Wessel and Flügge (38). Briefly, 200 μl supernatant were mixed with 800 μl methanol, followed by the addition of 200 μl chloroform and 600 μl water and vigorous mixing. The samples were centrifuged at 14,000 rcf for 5 min and the upper aqueous phase was carefully removed (the interphase contained precipitated proteins). Additional 600 μl methanol were added, liquids mixed and then centrifuged for 10 min at 14,000 rcf. The supernatant was removed and the final pellet was dissolved in a solution containing 6 M urea and 2 M thiourea prior dot blotting onto a PVDF membrane (described below) or stored at −20 °C for further use.

Mounted Sample Set—Microscope slides carrying H&E stained and unstained FFPE tissue sections (2–4 μm) were washed with xylene (3 × 2 min) followed by absolute ethanol (3 × 2 min), scraped off with a needle/razor blade and then transferred from the slide into a sample tube containing 4% SDS in 0.1 M Tris-HCl, pH 8.0 and 0.1 M DTT. The suspension was sonicated on ice (see above) and then further processed as described for the unmounted sections.

Laser Capture Microdissected Sample Sets—Tubes containing unstained, already deparaffinized washed cells (~1,000; ~5,000, and ~10,000), as well as H&E stained counter parts were incubated upside down to ensure capturing of microdissected samples usually located at the lid of the tube after the dissection procedure, for 30 min in 4% SDS in 0.1 M Tris-HCl, pH 8.0, 0.1 M DTT. Subsequently the samples were incubated in the same buffer for 60 min at 99 °C. Samples were then further processed as described for the unmounted sections.

A second set of laser capture microdissected tissue containing approx. 2000 cells per microdissection were obtained from three subsequent FFPE tissue sections of either hepatocellular carcinoma or surrounding nontumor tissue. Microdissected samples were treated as described above.

Frozen Sample Sets—Protein extraction of frozen tissues was done as described earlier (39). Briefly, liver tissue blocks were homogenized on ice using a IKA "T10 basic" homogenizer (Staufen, Germany) in lysis buffer (pH 7.4) containing 50 mM Tris-HCl, 0.1 M sodium chloride, 1 mM ethylenediaminetetraacetic acid and protease inhibitor mixture (Promega, Mannheim, Germany) and incubated for 20 min. The solution was then sonicated on ice using a tabletop Branson sonifier B-12 sonicator (Branson Sonic Power output control: 1.5; 3 × 10–30 s) and centrifuged at 2000 rcf for 20 min at room temperature. Supernatants were spotted directly onto PVDF membranes (see below) or stored at −20 °C.

PVDF Dot Blotting and N- *and* O*-glycan Release*—Extracted proteins were dot-blotted (frozen/FFPE tissue) onto a 0.2 μm pore size PVDF membrane (Millipore, Tullagreen, Ireland) and *N*- and *O*-glycans were sequentially released as described in detail previously (35, 36).

To assure that comparable protein amounts were used for the glycan release, dilutions series (1:2; 1:4; 1:8; 1:16; 1:20; 1:32) of proteins extracted from FFPE tissue sections (unmounted sections only) were prepared and spotted onto the membrane (data not shown). Spots exhibiting similar direct-blue 71 staining intensities compared with the fresh-frozen proteins were considered to contain comparable amounts of protein immobilized on the PVDF membranes and were used for subsequent glycan release.

Analysis of Released N- *and* O*-glycans Using Porous Graphitized Carbon Liquid Chromatography Electrospray Ionization Mass Spectrometry*—Following a final offline carbon desalting step as described previously (35) samples were dissolved in 10 μl MilliQ-water and 3 μl were injected for each LC-MS run. The PGC nanoLC setup was as follows: a PGC precolumn (HYPERCARB 5 μm, 30 × 0.32 mm, Thermo Fisher Scientific, Waltham, MA) and a PGC separation column (HYPERCARB 3 μm, 100 × 0.075 mm, Thermo Fisher Scientific) were installed in Ultimate 3000 UHPLC system (Dionex, Germering, Germany). The precolumn was equilibrated in buffer A (10 mM ammonium bicarbonate) and released glycans were loaded onto the precolumn for 5 min at 6 μl/min flow rate prior valve switching. The equilibration conditions for the separation column were 3% buffer B (60% ACN in 10 mM ammonium bicarbonate). After loading the released glycans onto the trapping column, a linear gradient was established using buffer B as follows: reduced *N*-glycans were separated using a linear gradient from 3% buffer B to 15.8% in 1 min before increasing to 40.3% buffer B over 49 min. *O*-glycans were analyzed using the same setup but applying a linear gradient from 2% to 35% buffer B over 33 min. The flow rate was set to 0.8 μl/min and the columns were held at a constant temperature of 40 °C. The LC was directly coupled to an amaZon speed ETD ion trap mass spectrometer equipped with a CaptiveSpray source (Bruker, Bremen, Germany) for online detection of glycans in negative ion mode. MS spectra were acquired in UltraScan mode within an *m/z* range of 380 - 1800; smart parameter setting (SPS) was set to *m/z* 900; ion charge control (ICC) to 40,000 and max. acquisition time to 200 ms.

MS/MS spectra were generated using collision induced dissociation over an *m/z* range from 100 - 2,500 on the three most abundant precursors applying an isolation width of *m/z* 3. The fragmentation cut-off was set to 27% with 100% fragmentation amplitude using the Enhanced SmartFrag option from 30–120% in 32 ms. ICC was set to 150,000.

Structure Determination and Relative Glycan Quantitation—*N*- and *O*-glycan structures were identified by manual screening of spectra and annotated, including isomeric structure elucidation, based on PGC retention time (35, 40–42), negative-ion mode fragmentation behavior (43–55), and biosynthesis pathways known from literature (56, 57). Nomenclature is based on Varki *et al.* (58). Representative MS/MS spectra for each identified glycan structure (if applicable) can be generated from the information given (*m/z*, intensity) in the Supplementary Material. Mass lists of fragment spectra were generated from raw data using DataAnalysis Version 4.1 (Bruker) with an absolute intensity threshold of 50 (no rel. threshold used), a S/N ratio of 1 and a peak width (FWHM (*m/z*)) of 0.1. Besides manual annotation, glycan product ion spectra were assigned using ProteinScape 4.0 (Bruker) using the GlycomeDB database or Glycoworkbench 2.1 (59). For ProteinScape searches, the following parameters were selected: Glycan type: *N*-glycan; Taxonomy: *Homo sapiens*; Derivatization: UND (underivatized); Reducing end: reduced; Ions: H+ up to 3 charges; Charge -: 1–3; MS tolerance: 0.6 Da; MS/MS tolerance: 0.6 Da; Mass type: monoisotopic; Fragmentation type: CID a b c x y z, cross-rings ≤1, cleavages ≤2. Thresholds were set at Score: ≥5%, Fragmentation coverage: ≥5% and Intensity coverage: ≥5%. ProteinScape glycan assignments were accepted if the score was ≥10. All assigned spectra and identified peaks are listed in the supplementary material.

Relative abundances of individual glycan structures were determined using the area under the curve (AUC) from the respective individual chromatographic traces (extracted ion chromatograms, EIC) of the corresponding monoisotopic precursors using QuantAnalysis software (Version 2.1, Bruker). The integration limits of all AUCs were checked and, if needed, adjusted manually. The sum of all detected and quantified glycan structures within a sample corresponded to 100% and the individual relative amounts were determined from the individual AUC values. Relative abundances were also calculated in relation to the highest peak when necessary. Note that a relative abundance of 1% was set as feasible threshold to take structures in consideration for quantitative changes in the course of this study.

Experimental Design and Statistical Rationale—We developed, optimized, and downscaled an analytical FFPE glycomics workflow for *N*- and *O*-glycans using hepatic specimens obtained from patients diagnosed with hepatocellular carcinoma (HCC) and selected for liver transplantation. One part of the tissue was immediately fractionated and frozen in liquid nitrogen (in the text referred to as *frozen tissue*) whereas the other part was subsequently FFPE-preserved (referred to as *FFPE tissue*). Glycans were released from proteins dot-blotted onto a PVDF membrane after extracted from tissue. Using clinical H&E stained and unstained tissue sections, the entire analytical workflow was developed and validated, minimal sample requirements evaluated and potential unintended artifacts induced by FFPE preservation, staining or antigen retrieval identified. The protocol was further optimized for minimal amounts of FFPE tissue (1,000; 5,000; 10,000 cells), selected by LCMs. The optimized protocol was then used with ~2,000 hepatocytes from HCC tissue and surrounding nontumor tissue (Fig. 1).

Statistical analyses of the relative abundances of the *N*- and *O*-glycans from different origins (*e.g.* frozen/FFPE or tumor/nontumor) are based on a linear model. Different sample sources were tested for equal suitability in glycomics analyses. Samples from different disease states were investigated for differences in relative abundances of glycans. The fold changes of the relative abundance of the compared samples and their respective *p* values were plotted in the shape of Volcano plots (see Supplementary Material). Oligosaccharide structures with a mean relative abundance of less than 0.3% were not plotted if that threshold was not reached in either of the compared groups. This was done for clarity and potential issues arising from not accurate quantitation of very small peak areas. The *p* values were corrected for multiple testing using the method of Benjamini and Hochberg (60). Changes in relative glycan abundances with a *p* value of less than 0.01 were regarded to be statistically significant. Unsupervised hierarchical cluster analysis was applied for data visualization in the form of heatmaps. The logarithmic relative abundance values were used to calculate the Euclidean distance matrix and

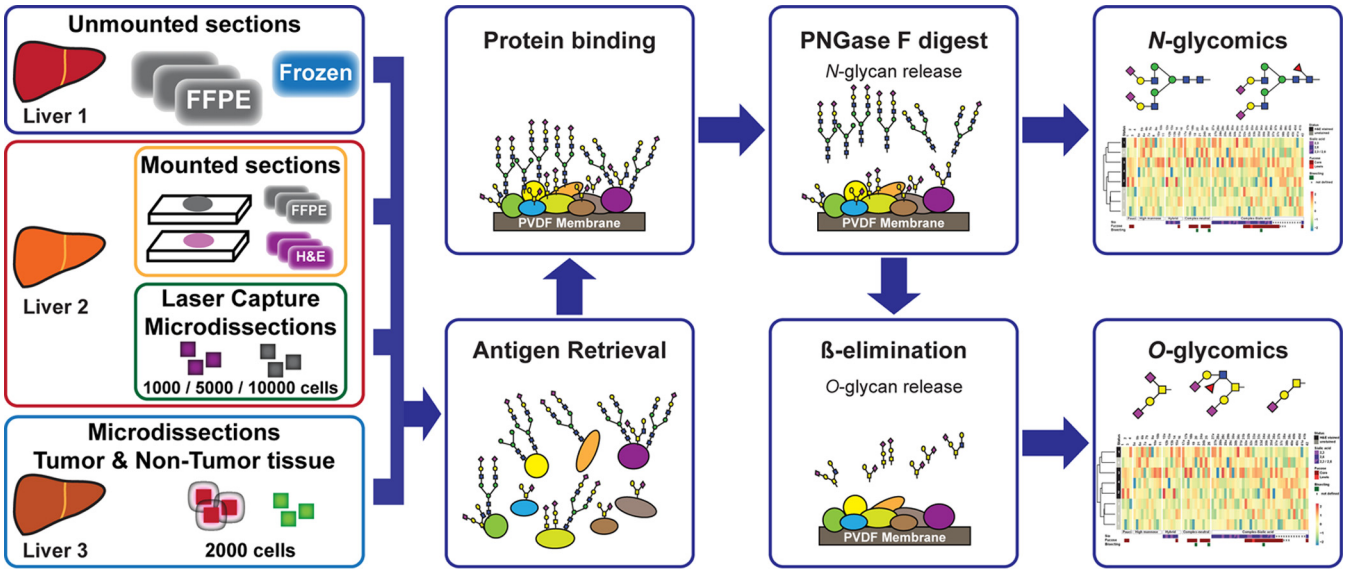

FIG. 1. **Overview on the FFPE-tissue workflow for clinical *N*- and *O*-glycomics.** Entire tissue blocks, slide-mounted tissue sections before or after H&E staining or micro-dissected tissue specimens provide clinical tissue sources. After antigen retrieval (glyco)proteins are immobilized onto PVDF membranes and *N*- and *O*-glycans are sequentially released for porous graphitized carbon nanoLC-ESI MS/MS based glycomics.

complete-linkage clustering in the sample dimension. Additionally, for plotting the values of each glycan structure were scaled to have mean zero and standard deviation one (*Z*-score normalization), except in Fig. 4*B*. For Fig. 2*A* a second stage of clustering was applied in the glycan dimension for each of the five main structural groups separately. The free software for statistical computing and graphics "R" (61) was used as data analysis environment. The code is available upon request.

RESULTS

Frozen and hepatic FFPE clinical tissue was used for extraction on *N*- and *O*-glycans. The analytical FFPE glycomics workflow was developed for whole tissue sections, further optimized for minimal sample amounts, including laser-derived microdissections, evaluated and potential unintended artifacts induced by sample preparation identified. Chloroform-methanol precipitation (38) prior glycoprotein immobilization on PVDF membranes (35) was found to be beneficial for the subsequent *N*- and *O*-glycan release as well as for PGC nanoLC-ESI MS/MS glycomics. This step removes excess SDS and other contaminant substances resulting in clearly reduced background contamination levels, better data quality and a clear sensitivity increase (data not shown). Comprehensive *N*- and *O*-glycome profiles were generally obtained from tissue slides down to 3 μm in thickness and a surface area of $\sim$15 mm^2.

Easy Cleavable Glycoepitopes Remain Intact During Preservation and Extraction—Once a highly sensitive *N*- and *O*-glycomics protocol for FFPE tissue material was established we compared the glycomes obtained from the different sources. The *N*-glycan base peak chromatograms (BPCs) acquired from representative FFPE and frozen tissue specimens appeared equivalent (supplemental material S1*A*). Among the ten most abundant compositions nine were identical between the two sample sources (Fig. 2*B*). Sialylated, complex biantennary ($\sim$66%) and fucosylated structures ($\sim$40%) were the most abundant *N*-glycans (Fig. 2*C*, supplemental material S1*G*). In total 74 different *N*-glycan structures (derived from 40 compositions) were detected in both, FFPE and frozen tissues (details in supplemental material S1*B*). The distribution of α2,6:α2,3 linked NeuAc residues on complex *N*-glycans was roughly 2:1. Fucose residues were mainly attached to the *N*-glycan core (35%) with just $\sim$5% of the hepatic *N*-glycome exhibiting Lewis type fucosylation (Fig. 2*C*, supplemental material S1*G*). The same glyco-epitopes were detected in similar amounts in both, FFPE and frozen samples, indicating that the preservation process and the sample preparation required for antigen retrieval did not affect any more readily cleavable glycoepitopes containing sialic acid or fucose residues (supplemental material S1*B*).

The hepatic *O*-glycome consisted of just eight different *O*-glycans present in six compositions (Fig. 2*D*, supplemental material S2*A*). These were exclusively of the core 1 and core 2 type with up to two NeuAc residues. In summary, these data confirmed that the FFPE preservation process and the antigen retrieval did not introduce any qualitative changes on the detectable *N*- and *O*-glycome.

Subtle Quantitative Glycome Differences Are Present Between Frozen and FFPE Specimens—Quantitative changes in the glycome are a major parameter determined in any disease related glycomics study. Therefore, we tested whether the quantitative glycome was similar between frozen and FFPE specimens. The detected *N*-glycans were categorized into global structure categories (Fig. 2*C*) and their relative quanti-

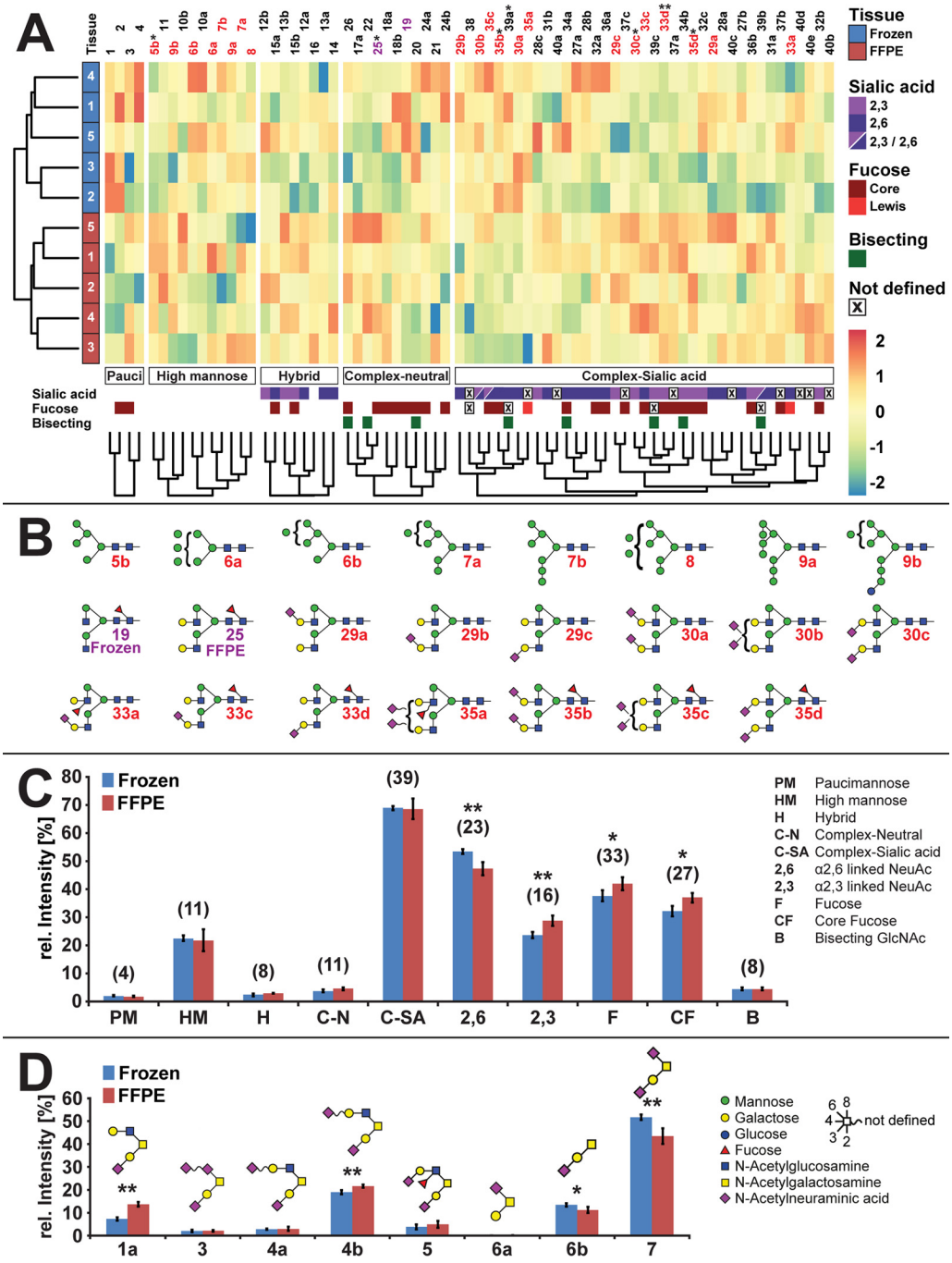

FIG. 2. **Comparison of *N*- and *O*-glycans released from unmounted FFPE tissue sections and matching frozen human hepatic tissue.** *A*, Heat map obtained after unsupervised clustering of the detected *N*-glycans generated from various technical replicates of the two sample sources. Detected *N*-glycan structures (the ten most abundant compositions are colored, see also supplemental material S7*A* for an overview) are represented by structure ID numbers on the top side of the heat map. The structure numbering refers to the respective IDs described in supplemental material S7*A*. Asterisks above numbers indicate the *p* value range obtained for statistically relevant differences between the starting materials (≤ 0.01 (**) or ≤ 0.05 (*)). The heat map is sorted according to different structure classes (dendrograms at the bottom of the heat map), whereas the different color boxes on the bottom provide additional structural information on the individual *N*-glycans (*e.g.* NeuAc or fucose linkage, presence of bisecting GlcNAc). The samples cluster according to sample origin (frozen and FFPE) because of differences in the relative intensity of mainly α2,3/α2,6 linked NeuAc residues. *B*, Structures are depicted for the ten most abundant *N*-glycan compositions (red label). Structure 19 and 25 (purple label) were the 10th most abundant composition in one sample source. *C*, Category comparison of the hepatic *N*-glycome obtained from frozen or FFPE starting material. Error bars represent the standard deviation determined from 5 technical replicates. The number of structures in each category is indicated above bars. *D*, Comparison of the hepatic *O*-glycome obtained from frozen or FFPE starting material. The structure numbering refers to the respective IDs described in Supplemental material 8a.

tative distribution assessed by an unsupervised hierarchical cluster analysis (Fig. 2*A*). These data indicated that mostly the levels of *N*-glycans carrying α2,3 linked NeuAc and/or fucose residues were slightly elevated in the FFPE tissue compared with frozen tissue (Fig. 2*A*, 2*C*). In particular, complex sialylated core fucosylated *N*-glycans (*e.g.* IDs 30c, 33d and 35d) showed higher abundances in FFPE tissue samples, whereas α2,6 NeuAc carrying *N*-glycans were slightly elevated in frozen tissue (Fig. 2*A*, 2*C*; supplemental material S1*G,* S1*H*). The unsupervised cluster analysis also indicated differences between frozen and FFPE tissue for some paucimannnosidic and complex neutral type *N*-glycans, however, further statistically relevant differences were confirmed only for structures 5b and 25 (Fig. 2*A*, 2*B*, see also supplemental Fig. S1). These data emphasize that a direct comparison between frozen and FFPE derived starting material should be avoided as the tissue source already results in minor, though statistically relevant glycome differences, which might lead to false positive results in differential studies. Despite these no other global trends indicating destruction or discrimination of particular more readily cleavable monosaccharides such as fucose or sialic acid residues were observed. Furthermore, no unintended chemical modifications could be detected, further supporting the principal usability of FFPE conserved specimens for glyco-biomarker studies.

Some quantitative differences between the different sample sources were also found for the *O*-glycome. The singly and doubly sialylated core 2 type structures 1a ($Hex_2HexNAc_2$ NeuAc) and 4b ($Hex_2HexNAc_2NeuAc_2$) were more prominent in FFPE samples whereas the levels of structures 7 ($HexHexNAcNeuAc_2$) and 6b (HexHexNAcNeuAc) were less abundant in FFPE samples. Other structures present above a relative abundance of 1% did not show any detectable quantitative changes (Fig. 2*D*). Based on these results we concluded that for disease signature evaluation a direct comparison between frozen and FFPE tissues should be avoided as different starting materials obviously mimic statistically relevant signatures in clinical glycomics studies.

Glass Slide Mounted and H&E Stained Tissue Specimens Provide Suitable Sources for Clinical N- *and* O*-glycomics*—The mounting of FFPE tissue sections onto glass slides and H&E tissue staining represent standard procedures in every pathology laboratory. We evaluated whether FFPE tissue sections that underwent these procedures are also suitable for clinical *N*- and *O*-glycomics. PGC nanoLC-ESI MS/MS glycomics performed on mounted FFPE preserved hepatic tissue sections (both, H&E stained and unstained) resulted in the detection of 77 *N*-glycan and 9 *O*-glycan structures, which was in good agreement with the results obtained for the unmounted material (Fig. 3*A*–3*C*, supplemental material S3*A* and S4*A*). Statistics indicated a significant difference for paucimannose type structures between untreated and H&E stained slides (Fig. 3*B*), however, as these four structures amount only ~2% of relative intensity, the minor individual tissue section differences could also cause the detected differences. The similar results obtained for essentially all *N*- and *O*-glycans from H&E stained and unstained tissue sections indicated that the staining method did not affect glycan integrity and antigen retrieval (Fig. 3*A*–3*C*, supplemental material S3*A,* S3*D* and S4*A*, S4*D*). These data also clearly demonstrated that glycomics information can be obtained from the very same material used for pathological examinations.

One Thousand Cells Are Sufficient for Composition Glycomics—LCM provides a unique possibility to selectively isolate areas of interest for subsequent glycomics studies. However, as this approach inevitable yields just small amounts of tissue, we evaluated the minimum number of cells required to still obtain a basic glycan profile. Approximately 1000, 5000 and 10,000 hepatocytes were isolated from unstained and H&E stained FFPE tissue sections for glycan profiling (Fig. 4*A*, 4*B*). In order to remain comparable with the analyses described above, also just 1/3 of the sample was actually used for a single PGC nanoLC-ESI MS/MS analysis despite the low amount of starting material.

We succeeded in obtaining basic *N*- and *O*-glycan profiles from as low as 1000 cells (Fig. 4*A*, 4*B*, supplemental material S3*K,* S4*G*). The detected signal intensities were low and just 25 out of 71 detected *N*-glycans met our stringent quantitation criteria. MS/MS based identification was successful for 20 out of 71 structures (38 and 50 out of 71 for 5000 and 10,000 cells, respectively, supplemental material S3*K*), with the residual being assigned based on retention time, precursor mass and hepatic glycome data acquired during this project. Four out of eight *O*-glycans could also be quantified from the 1000 cells starting material (supplemental material S4*G*). Even though glycan profiles were obtained from as low as 1000 cells, this amount was considered to be insufficient for reliable quantitative clinical glycomics. In particular, lower abundant structures could not be reliably quantified when starting from 1000 cells, making it very difficult to reliably detect subtle glycome changes. The use of higher cell numbers ($\geq$2000) provided in general reliable quantitative glycome profiling data (Fig. 4*A*, 4*B*). These results encouraged us to further pursue the LCM route and validate the usability of microdissection to complement histopathology with glycomics using hepatic cellular carcinoma tissue sections in a proof of principle study.

Spatial Insights into Hepatocellular Carcinoma N- *and* O*-glycome Using Laser-capture Microdissection*—Associating the glycome with microscopically visible tissue features provides a key requirement to exactly determine disease associated glycan signatures. Tumor tissue micro-heterogeneity, however, represents a major obstacle in tissue preparation for glycan profiling as the presence of nontumor related cells can mask tumor specific glycosylation features (22). LCM can help overcome this obstacle as it provides the possibility to specifically select tissue areas of interest that are also cross-

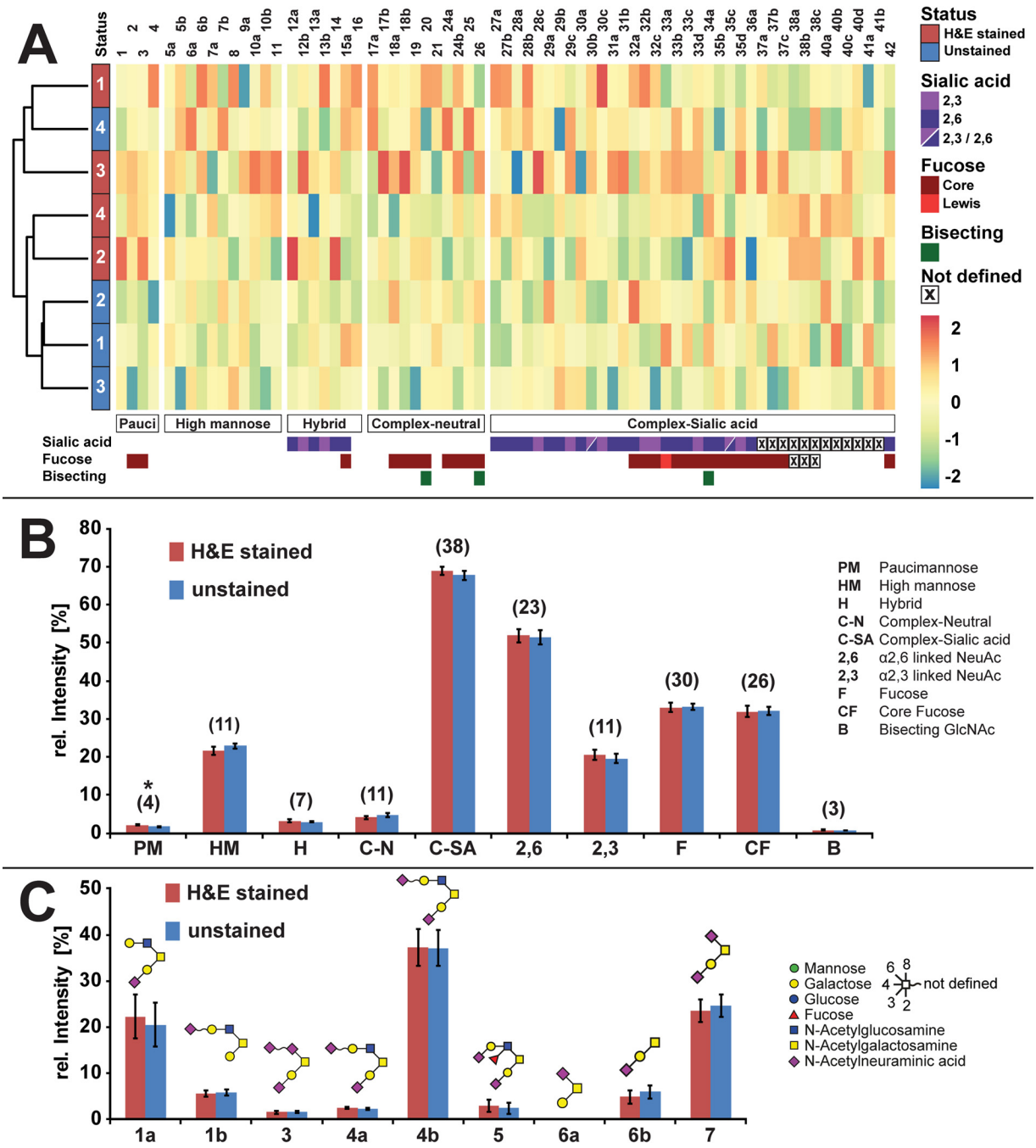

FIG. 3. **Comparison of the hepatic *N*- and *O*-glycome obtained from unstained and hematoxylin and eosin (H&E) stained FFPE tissue sections.** *A*, Heat map obtained after unsupervised clustering of the detected *N*-glycans, sorted according to *N*-glycan categories. The differences in relative *N*-glycan abundances indicated by the clustering analyses between the H&E stained and untreated FFPE sections are smaller than the methodological and individual slide specific differences as indicated by the fact that no clear sample source derived clustering was obtained. Detected *N*-glycan structures are represented by structure ID numbers (for details see also supplemental material S7*A*) on top of the heat map. The heat map is sorted according to different structure classes (bottom of the heat map), whereas the different color boxes on the bottom provide additional structural information on the individual *N*-glycans (*e.g.* NeuAc or fucose linkage, presence of bisecting GlcNAc). *B*, Category comparison of the hepatic *N*-glycome obtained from unstained (blue) or H&E stained (red) FFPE tissue sections. Error bars represent the standard deviation determined from 4 technical replicates. The number of structures in each category is indicated above bars. The asterisks indicate the *p* value range obtained for statistically relevant differences between the starting materials (≤ 0.05 (*)). *C*, Comparison of the hepatic *O*-glycome obtained from unstained (blue) or H&E stained (red) FFPE tissue sections. Error bars represent the standard deviation determined from the analysis of 5 technical replicates.

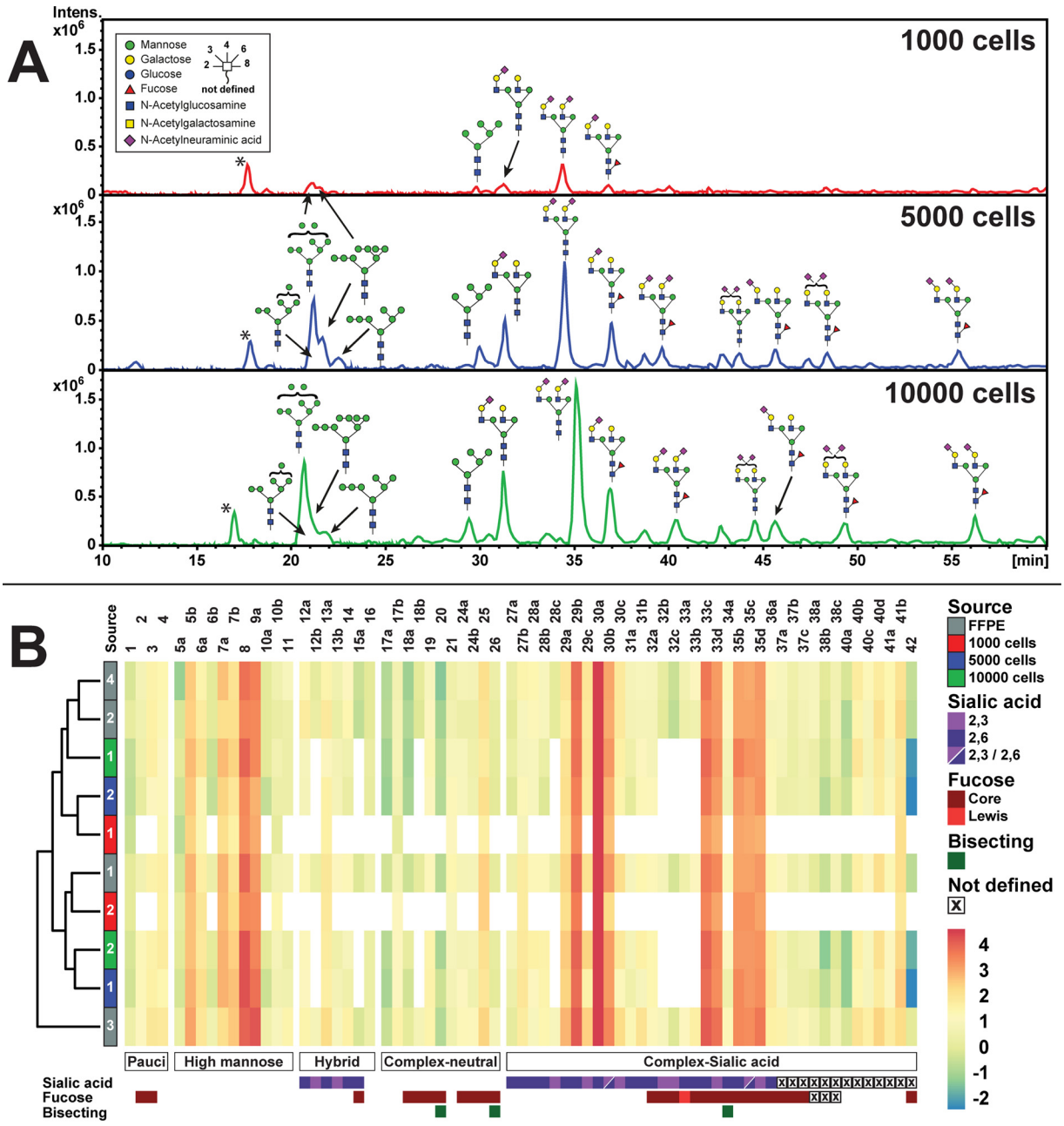

FIG. 4. ***N*-glycome determined from hepatocytes (1,000; 5,000 and 10,000 cells) microdissected from H&E stained FFPE tissue slides and analyzed by porous graphitized carbon nanoLC-ESI MS/MS glycomics.** *A*, *N*-glycan base peak chromatograms (BPC) obtained from 1,000; 5,000 and 10,000 cells isolated from H&E stained FFPE tissue sections by laser capture microdissection. The intensity for all BPCs was normalized to the most intense sample (10,000 cells). The major *N*-glycan structures have been indicated at their respective retention time in the BPC. The asterisk indicates a nonglycan contamination signal. *B*, Heat map obtained after unsupervised hierarchical clustering of the *N*-glycans detected from 1000; 5000 and 10,000 cells compared with the ones obtained from entire FFPE tissue sections and sorted according to major structure categories. Detected *N*-glycan structures are represented by structure ID numbers (for details see also supplemental material S7*A*) on top of the heat map. The heat map is sorted according to different structure classes (bottom of the heat map), whereas the different color boxes on the bottom provide additional structural information on the individual *N*-glycans (*e.g.* NeuAc or fucose linkage, presence of bisecting GlcNAc). Despite the fact that with lower cell numbers less *N*-glycans were detectable (indicated by the white boxes), no cell number associated clustering occurred, indicating that the overall profile remains comparable independent of the cell number and that the microdissection itself does not alter the glycan profile.

validated by classical pathology diagnoses. In addition, this technique provides the opportunity to gain access to nontumor tissue parts from the very same patient reducing the factor of individual glycosylation heterogeneity. We applied this technique to gain further insights into the individual glycosylation signatures of HCC.

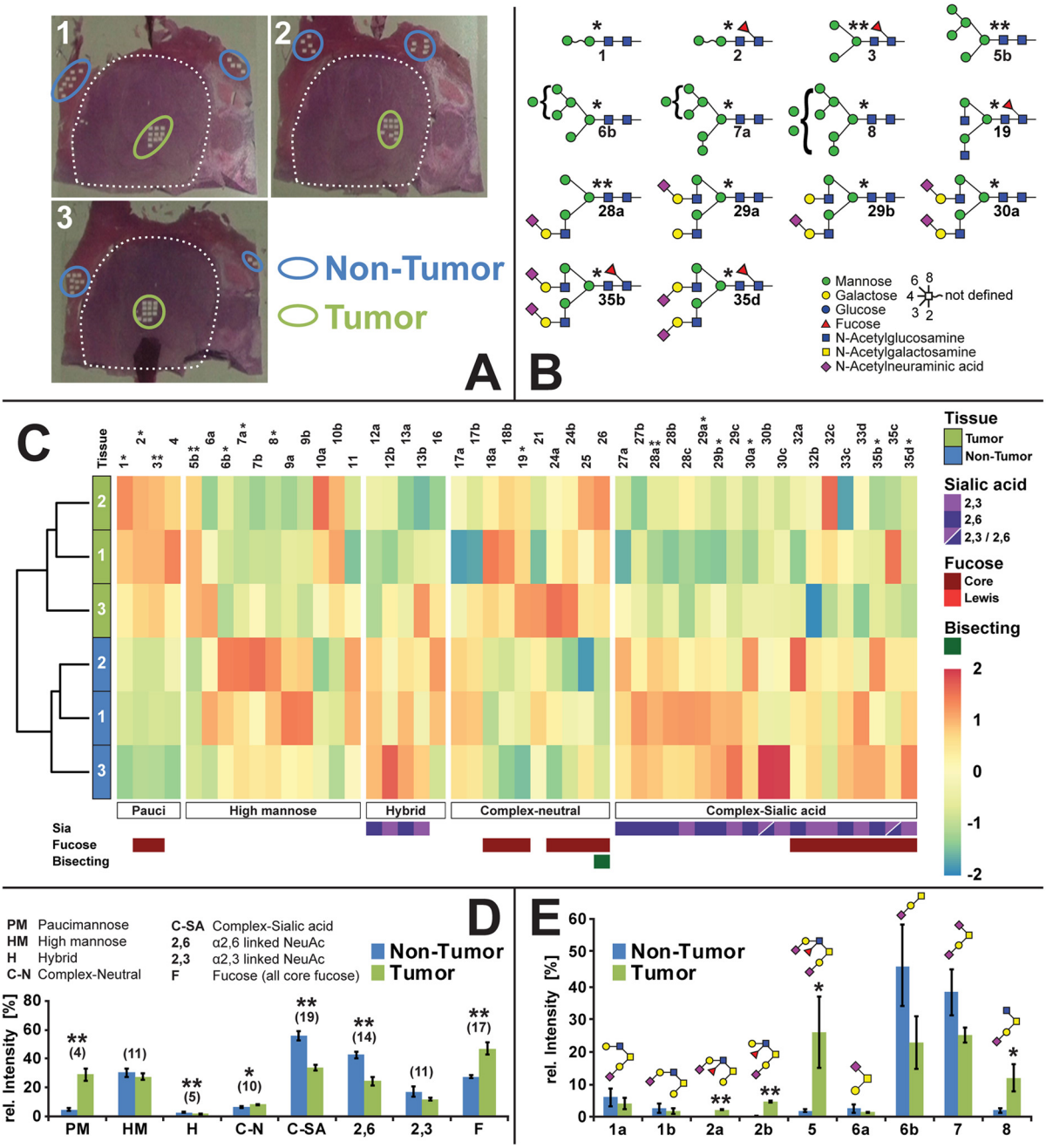

FIG. 5. ***N*- and *O*-glycome of hepatocellular carcinoma (HCC) and noncancer hepatic tissue (NC).** *A*, Representative image of FFPE preserved tissue sections of HCC used for spatial isolation of HCC cells and surrounding noncancerous tissue by laser capture microdissection. The respective areas used for the analyses are labeled as indicated. *B*, Overview on the *N*-glycan structures exhibiting the largest expression level changes between HCC and NC tissue including their structure IDs as listed in supplemental material S7*A*. The number of asterisks indicate the *p* value range obtained for statistically relevant differences between the starting materials (≤ 0.01 (**) or ≤ 0.05 (*)). *C*, Heat map obtained after unsupervised hierarchical clustering of the *N*-glycans detected from ~2,000 cells of HCC and NC hepatic tissue and sorted according to major structure categories. Detected *N*-glycan structures are represented by structure ID numbers (for details see also supplemental material S7*A*) on top of the heat map. The heat map is sorted according to different structure classes (bottom of the heat map), whereas the different color boxes on the bottom provide additional structural information on the individual *N*-glycans (*e.g.* NeuAc or fucose linkage, presence of bisecting GlcNAc). Based on the *N*-glycome, HCC and NC tissue cluster in distinct classes. Paucimannose type and α2,6 NeuAc carrying *N*-glycans show the highest alterations between these two tissue types. *D*, Category comparison of the HCC and NC *N*-glycomes. The number of structures in each category is indicated above bars. Error bars represent standard deviation determined from 3 technical replicates. *E*, Comparison of HCC and NC *O*-glycomes obtained from the very same material the *N*-glycomes were obtained. Sialyl Lewis X epitopes present on core 2 type *O*-glycans show a significant increase in HCC tissue, whereas core 1 type *O*-glycan levels are reduced.

N- and *O*-glycan profiles were determined from ~2000 cells isolated by the LCM method (Fig. 5*A*). The glycome of nontumor tissue was comparable to the ones obtained for different liver samples described above (supplemental material S10). Significant global glycome changes were observed in the isolated HCC cells for various *N*-glycans of the paucimannose and core fucosylated type, but also for hybrid as well as neutral and α2,6 sialylated *N*-glycans (Fig. 5*B*–5*D*). Though high mannose type glycans appeared unaltered as a group, the levels of individual structures (Man8, Man7 and Man6, IDs: 8, 7a, 6b, respectively) were significantly decreased, whereas Man5 (ID: 5b) showed an opposite trend (Fig. 5*C*, and supplemental material S5*B*). The most striking changes were detected for paucimannosidic structures such as $Hex_2HexNAc_2$ Fuc (ID: 2) and $Hex_3HexNAc_2Fuc$ (ID: 3) and the biantennary, doubly α2,6 sialylated structure (ID: 30a, Fig. 5*B*, 5*C*).

The *O*-glycome obtained from the very same microdissected tumor tissue specimens showed more complex core 2 type structures carrying Lewis X and sialyl Lewis X glycoepitopes that shifted toward shorter core 1 type *O*-glycans in the noncancerous surrounding cells (Fig. 5*E*). Similar core 2 *O*-glycans have previously been described in numerous tumor types and have been linked to increased tumor survival and metastasis by modulating the immune response (62, 63). As the hepatic *O*-glycome is significantly less complex compared with the *N*-glycome, in future *O*-glycans might present a useful and simpler alternative in the context of HCC tissue differentiation.

DISCUSSION

In principle glycans have been isolated from FFPE tissue sections already previously (31–33). Despite these earlier reports we were, however, not able to find satisfying answers to numerous crucial questions. (1) Are all glyco-epitopes quantitatively and qualitatively preserved during the preservation and antigen-retrieval procedures? (2) What is the minimum sample amount required to obtain a representative glycome? (3) Is glycan integrity and recovery still given even after H&E staining?

To address these questions, we developed and applied a novel PGC nanoLC-ESI MS/MS glycomics approach for qualitative and relative quantitative *N*- and *O*-glycomics of clinical FFPE tissue sections and even LCM-enriched tissue specimens. Our results showed that unstained or H&E stained FFPE tissue sections represent well suited sources for clinical glycomics. In a proof of principle experiment we analyzed *N*- and *O*-glycans from hepatic tumor and surrounding nontumor tissue derived from the very same tissue section and patient. Using laser capture microdissection patient-derived individual glycome variations were reduced and the results provided a more precise view on the specific and individual cancer tissue glyco-signatures as tumor and control samples were also derived from spatially close areas. This approach allowed an in-depth characterization of the hepatic *N*- and *O*-glycome from single tissue specimens including differentiation and relative quantitation of structure isomers (Fig. 6).

Our results clearly emphasize that similar tissue specimen treatment is imperative for glyco-biomarker studies. Minor though significant differences were detected when the glycome of frozen starting material was compared with the FFPE-derived profile. Inevitably the different starting conditions required different initial tissue homogenization and protein extraction procedures. Thus, most likely specific proteins were lost and/or insoluble in either one of the procedures, subsequently resulting in the lack of specific glycoproteins. The FFPE sections were also derived from a spatially narrower tissue fraction compared with the frozen material, thus a differential spatial glycan distribution as reported previously by MALDI imaging experiments (31, 64) could also contribute to the observed quantitative changes. Nevertheless, in the initial method development several larger tissue sections were combined, making spatial distribution differences less a likely option for the observed differences.

Turiak *et al.* also reported differences in the number and relative abundances of *N*-glycans released from frozen and FFPE murine liver tissue (13 *versus* 14 compositions) (25). In their interesting integrated omics approach they identify proteins and profile glycosaminoglycans and *N*-glycans from the same FFPE-slide. Nevertheless, in their workflow reliable detection and quantitation of released *N*-glycans required six sequential sections (10 μm thick, ~2 mm^2 in size) to be combined, whereas we consistently identified 63 *N*-glycans and 7 *O*-glycans from 5000 cells.

In comparison to a recent *N*-glycan MALDI-imaging study on HCC including two patients overall just 17 of the reported 33 *N*-glycans qualitatively overlapped with our results (64). Whereas in our data paucimannosidic *N*-glycans in particular showed the largest differences (Fig. 5*B*–5*D*), Powers *et al.* (64) reported the largest differences for high mannose type and selected complex, nonsialylated *N*-glycans. Because of the *m/z* cut-off used in their study, paucimannosidic *N*-glycans eluded their detection. Nevertheless, the observed differences are possibly also a reflection of individual patient variability. The unavoidable influence of this factor on such clinical glycomics studies is further supported by the fact that Powers *et al.* reported contradicting results for some high mannose structures in an earlier, similar study conducted on 16 patients (65). Whereas a decrease of Man8 in HCC tissues is supported by data presented in this work and by two independent reports from Powers *et al.* (65) and Nie *et al.* (66), the follow up study from Powers and co-workers reported an increase in Man8 in HCC tissues (64). This example clearly shows that future biomarker oriented studies require both large sample cohorts and orthogonal approaches to differentiate individual patient glycan heterogeneity from possible method artifacts and real cancer signatures. This will be crucial to identify glycan signatures with the potential to support

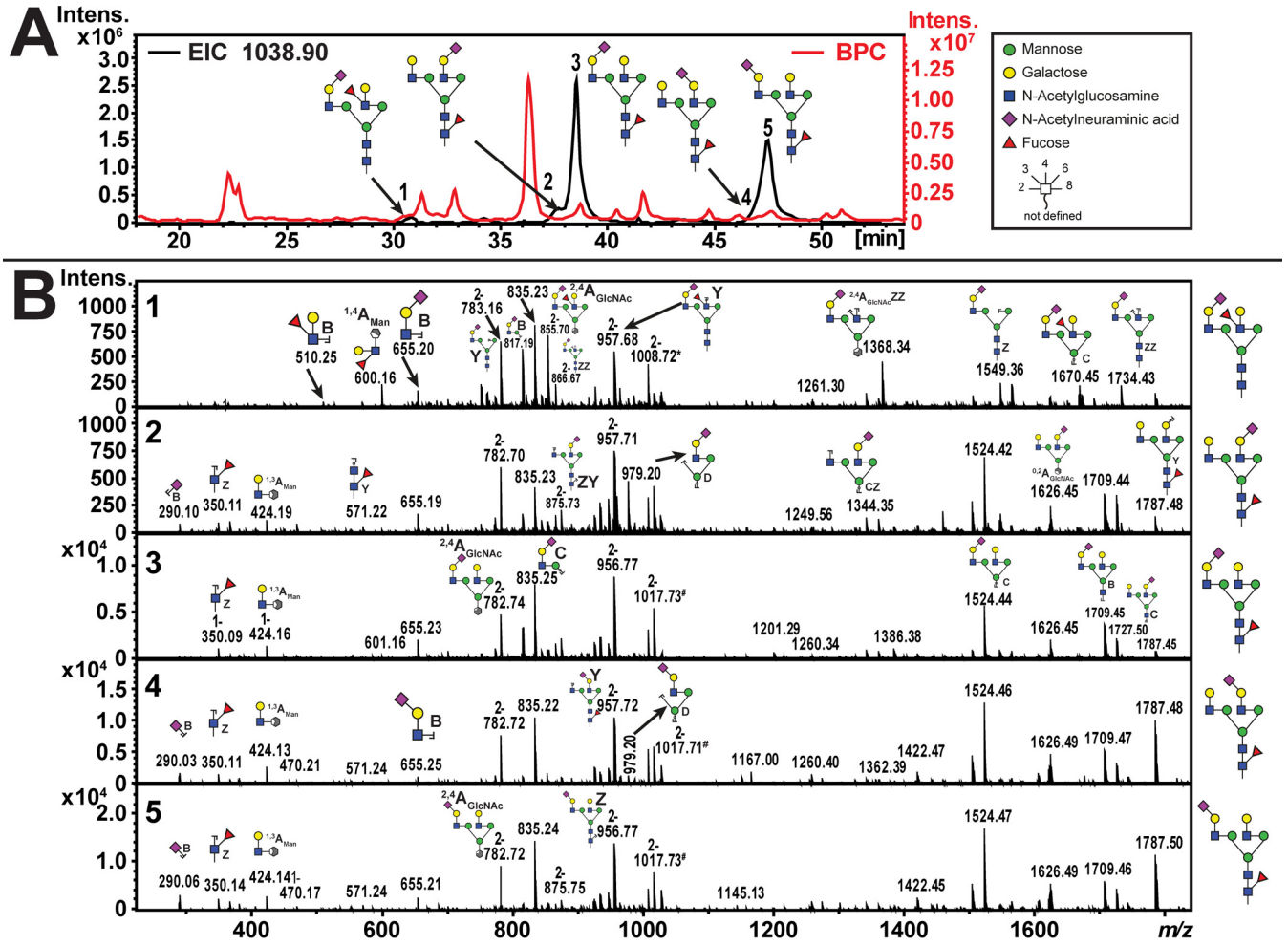

FIG. 6. **Example for structure identification using porous graphitized carbon nano LC-ESI MS/MS.** *A*, Base peak chromatogram (BPC, red trace) representing the *N*-glycome obtained from FFPE preserved hepatic tissue. Extracted ion chromatogram (EIC, black trace) of an example *N*-glycan ($Hex_5HexNAc_4NeuAcFuc$, $[M-2H]^{2-}$ = 1038.9 Da) that is present in five different structure isomers. *B*, Individual product-ion spectra of the five $Hex_5HexNAc_4NeuAcFuc$ isomers enabling differentiation and relative quantitation of the various *N*-glycan isomers.

histopathology and also future personalized cancer diagnostics or therapies (6).

The here presented liver *O*-glycome showed a low structure diversity. To date just very few data is available on the liver tissue *O*-glycome, and our results agree well with the data provided by the Consortium of functional glycomics that also reported a similar low *O*-glycan structure diversity in human liver (see glycan structure database for human tissue on: www.functionalglycomics.org).

The here presented method is generally applicable to any tissue type and opens novel opportunities to study protein *N*- and *O*-glycosylation including isobaric structure differentiation directly from histopathologically examined tissue specimens orthogonal to MALDI imaging techniques. Furthermore, our results unlock the potential of FFPE tissue as a valuable and easily accessible source for future clinical glyco-biomarker studies.

Acknowledgments—We thank Dr. Ursula Neu for fruitful discussion of the manuscript.

* This work was supported by the Max Planck Society and European Union (Seventh Framework Program "Glycoproteomics" project, grant number PCIG09-GA-2011-293847, IBD-BIOM project, grant number 305479).

S This article contains supplemental material.

‡‡ To whom correspondence should be addressed: Max Planck Institute of Colloids and Interfaces, Department of Biomolecular Systems, 14424 Potsdam, Germany. Tel.: +49-30-838 59306; Fax: +49-30-838 459306; E-mail: daniel.kolarich@mpikg.mpg.de.

§§ Present address: Institute for Glycomics, Gold Coast Campus, Griffith University, Queensland, 4222, Australia, Email: d.kolarich@griffith.edu.au, Telephone: +61-7-5552 7026.

REFERENCES

1. Moremen, K. W., Tiemeyer, M., and Nairn, A. V. (2012) Vertebrate protein glycosylation: diversity, synthesis and function. *Nat. Rev. Mol. Cell Biol.* **13,** 448–462

2. Held, W., and Mariuzza, R. A. (2011) Cis-trans interactions of cell surface receptors: biological roles and structural basis. *Cell. Mol. Life Sci.* **68,** 3469–3478
3. Croci, D. O., Cerliani, J. P., Dalotto-Moreno, T., Mendez-Huergo, S. P., Mascanfroni, I. D., Dergan-Dylon, S., Toscano, M. A., Caramelo, J. J., Garcia-Vallejo, J. J., Ouyang, J., Mesri, E. A., Junttila, M. R., Bais, C., Shipp, M. A., Salatino, M., and Rabinovich, G. A. (2014) Glycosylation-dependent lectin-receptor interactions preserve angiogenesis in anti-VEGF refractory tumors. *Cell* **156,** 744–758
4. Marth, J. D., and Grewal, P. K. (2008) Mammalian glycosylation in immunity. *Nat. Rev. Immunol.* **8,** 874–887
5. Stowell, S. R., Ju, T., and Cummings, R. D. (2015) Protein glycosylation in cancer. *Ann. Rev. Pathol.* **10,** 473–510
6. Almeida, A., and Kolarich, D. (2016) The promise of protein glycosylation for personalised medicine. *Biochim. Biophys. Acta* **1860,** 1583–1595
7. Kristic, J., Vuckovic, F., Menni, C., Klaric, L., Keser, T., Beceheli, I., Pucic-Bakovic, M., Novokmet, M., Mangino, M., Thaqi, K., Rudan, P., Novokmet, N., Sarac, J., Missoni, S., Kolcic, I., Polasek, O., Rudan, I., Campbell, H., Hayward, C., Aulchenko, Y., Valdes, A., Wilson, J. F., Gornik, O., Primorac, D., Zoldos, V., Spector, T., and Lauc, G. (2014) Glycans are a novel biomarker of chronological and biological ages. *J. Gerontol. A Biol. Sci. Med. Sci.* **69,** 779–789
8. Knezevic, A., Gornik, O., Polasek, O., Pucic, M., Redzic, I., Novokmet, M., Rudd, P. M., Wright, A. F., Campbell, H., Rudan, I., and Lauc, G. (2010) Effects of aging, body mass index, plasma lipid profiles, and smoking on human plasma N-glycans. *Glycobiology* **20,** 959–969
9. Pucic, M., Knezevic, A., Vidic, J., Adamczyk, B., Novokmet, M., Polasek, O., Gornik, O., Supraha-Goreta, S., Wormald, M. R., Redzic, I., Campbell, H., Wright, A., Hastie, N. D., Wilson, J. F., Rudan, I., Wuhrer, M., Rudd, P. M., Josic, D., and Lauc, G. (2011) High throughput isolation and glycosylation analysis of IgG-variability and heritability of the IgG glycome in three isolated human populations. *Mol. Cell. Proteomics* **10**, M111 010090
10. Fuster, M. M., and Esko, J. D. (2005) The sweet and sour of cancer: glycans as novel therapeutic targets. *Nat. Rev. Cancer* **5,** 526–542
11. Dube, D. H., and Bertozzi, C. R. (2005) Glycans in cancer and inflammation (mdash) potential for therapeutics and diagnostics. *Nat. Rev. Drug Discov.* **4,** 477–488
12. Christiansen, M. N., Chik, J., Lee, L., Anugraham, M., Abrahams, J. L., and Packer, N. H. (2014) Cell surface protein glycosylation in cancer. *Proteomics* **14,** 525–546
13. Miwa, H. E., Song, Y., Alvarez, R., Cummings, R. D., and Stanley, P. (2012) The bisecting GlcNAc in cell growth control and tumor progression. *Glycoconj. J.* **29,** 609–618
14. Adamczyk, B., Tharmalingam, T., and Rudd, P. M. (2012) Glycans as cancer biomarkers. *Biochim. Biophys. Acta* **1820,** 1347–1353
15. Wuhrer, M. (2007) Glycosylation profiling in clinical proteomics: heading for glycan biomarkers. *Expert Rev. Proteomics* **4,** 135–136
16. Theodoratou, E., Campbell, H., Ventham, N. T., Kolarich, D., Pucic-Bakovic, M., Zoldos, V., Fernandes, D., Pemberton, I. K., Rudan, I., Kennedy, N. A., Wuhrer, M., Nimmo, E., Annese, V., McGovern, D. P., Satsangi, J., and Lauc, G. (2014) The role of glycosylation in IBD. *Nature reviews. Gastroenterol.Hepatol.* **11,** 588–600
17. Abbott, K. L., Lim, J. M., Wells, L., Benigno, B. B., McDonald, J. F., and Pierce, M. (2010) Identification of candidate biomarkers with cancer-specific glycosylation in the tissue and serum of endometrioid ovarian cancer patients by glycoproteomic analysis. *Proteomics* **10,** 470–481
18. Chen, C. L., Chung, T., Wu, C. C., Ng, K. F., Yu, J. S., Tsai, C. H., Chang, Y. S., Liang, Y., Tsui, K. H., and Chen, Y. T. (2015) Comparative tissue proteomics of microdissected specimens reveals novel candidate biomarkers of bladder cancer. *Mol. Cell. Proteomics* **14,** 2466–2478
19. Fischer, A. H., Jacobson, K. A., Rose, J., and Zeller, R. (2008) Hematoxylin and eosin staining of tissue and cell sections. *CSH Protoc.* 2008, pdb prot4986
20. Magdeldin, S., and Yamamoto, T. (2012) Toward deciphering proteomes of formalin-fixed paraffin-embedded (FFPE) tissues. *Proteomics* **12,** 1045–1058
21. Ostasiewicz, P., Zielinska, D. F., Mann, M., and Wisniewski, J. R. (2010) Proteome, phosphoproteome, and N-glycoproteome are quantitatively preserved in formalin-fixed paraffin-embedded tissue and analyzable by high-resolution mass spectrometry. *J. Proteome Res.* **9,** 3688–3700
22. de Gramont, A., Watson, S., Ellis, L. M., Rodon, J., Tabernero, J., de Gramont, A., and Hamilton, S. R. (2015) Pragmatic issues in biomarker evaluation for targeted therapies in cancer. *Nat. Rev. Clin. Oncol.* **12,** 197–212
23. Klopfleisch, R., Weiss, A. T., and Gruber, A. D. (2011) Excavation of a buried treasure–DNA, mRNA, miRNA and protein analysis in formalin fixed, paraffin embedded tissues. *Histol. Histopathol.* **26,** 797–810
24. Casadonte, R., and Caprioli, R. M. (2011) Proteomic analysis of formalin-fixed paraffin-embedded tissue by MALDI imaging mass spectrometry. *Nat. Protoc.* **6,** 1695–1709
25. Turiak, L., Shao, C., Meng, L., Khatri, K., Leymarie, N., Wang, Q., Pantazopoulos, H., Leon, D. R., and Zaia, J. (2014) Workflow for combined proteomics and glycomics profiling from histological tissues. *Anal. Chem.* **86,** 9670–9678
26. Serth, J., Kuczyk, M. A., Paeslack, U., Lichtinghagen, R., and Jonas, U. (2000) Quantitation of DNA extracted after micropreparation of cells from frozen and formalin-fixed tissue sections. *Am. J. Pathol.* **156,** 1189–1196
27. Roberts, L., Bowers, J., Sensinger, K., Lisowski, A., Getts, R., and Anderson, M. G. (2009) Identification of methods for use of formalin-fixed, paraffin-embedded tissue samples in RNA expression profiling. *Genomics* **94,** 341–348
28. Kelly, A. D., Breitkopf, S. B., Yuan, M., Goldsmith, J., Spentzos, D., and Asara, J. M. (2011) Metabolomic profiling from formalin-fixed, paraffin-embedded tumor tissue using targeted LC/MS/MS: application in sarcoma. *PLoS ONE* **6,** e25357
29. van Wijk, X. M., Vallen, M. J., van de Westerlo, E. M., Oosterhof, A., Hao, W., Versteeg, E. M., Raben, J., Wismans, R. G., Smetsers, T. F., Dijkman, H. B., Schalkwijk, J., and van Kuppevelt, T. H. (2012) Extraction and structural analysis of glycosaminoglycans from formalin-fixed, paraffin-embedded tissues. *Glycobiology* **22,** 1666–1672
30. Toghi Eshghi, S., Yang, S., Wang, X., Shah, P., Li, X., and Zhang, H. (2014) Imaging of N-linked glycans from formalin-fixed paraffin-embedded tissue sections using MALDI mass spectrometry. *ACS Chem. Biol.* **9,** 2149–2156
31. Gustafsson, O. J., Briggs, M. T., Condina, M. R., Winderbaum, L. J., Pelzing, M., McColl, S. R., Everest-Dass, A. V., Packer, N. H., and Hoffmann, P. (2015) MALDI imaging mass spectrometry of N-linked glycans on formalin-fixed paraffin-embedded murine kidney. *Anal. Bioanal. Chem.* **407,** 2127–2139
32. Dwek, M. V., Brooks, S. A., Streets, A. J., Harvey, D. J., and Leathem, A. J. (1996) Oligosaccharide release from frozen and paraffin-wax-embedded archival tissues. *Anal. Biochem.* **242,** 8–14
33. Satomaa, T., Heiskanen, A., Leonardsson, I., Angstrom, J., Olonen, A., Blomqvist, M., Salovuori, N., Haglund, C., Teneberg, S., Natunen, J., Carpen, O., and Saarinen, J. (2009) Analysis of the human cancer glycome identifies a novel group of tumor-associated N-acetylglucosamine glycan antigens. *Cancer Res.* **69,** 5811–5819
34. Furukawa, J., Piao, J., Yoshida, Y., Okada, K., Yokota, I., Higashino, K., Sakairi, N., and Shinohara, Y. (2015) Quantitative O-Glycomics by Microwave-Assisted beta-Elimination in the Presence of Pyrazolone Analogues. *Anal. Chem.* **87,** 7524–7528
35. Jensen, P. H., Karlsson, N. G., Kolarich, D., and Packer, N. H. (2012) Structural analysis of *N*- and *O*-glycans released from glycoproteins. *Nat. Protoc.* **7,** 1299–1310
36. Kolarich, D., Windwarder, M., Alagesan, K., and Altmann, F. (2015) Isomer-specific analysis of released N-glycans by LC-ESI MS/MS with porous graphitized carbon. *Methods Mol. Biol.* **1321,** 427–435
37. York, W. S., Agravat, S., Aoki-Kinoshita, K. F., McBride, R., Campbell, M. P., Costello, C. E., Dell, A., Feizi, T., Haslam, S. M., Karlsson, N., Khoo, K. H., Kolarich, D., Liu, Y., Novotny, M., Packer, N. H., Paulson, J. C., Rapp, E., Ranzinger, R., Rudd, P. M., Smith, D. F., Struwe, W. B., Tiemeyer, M., Wells, L., Zaia, J., and Kettner, C. (2014) MIRAGE: the minimum information required for a glycomics experiment. *Glycobiology* **24,** 402–406
38. Wessel, D., and Flugge, U. I. (1984) A method for the quantitative recovery of protein in dilute solution in the presence of detergents and lipids. *Anal. Biochem.* **138,** 141–143
39. Lee, A., Kolarich, D., Haynes, P. A., Jensen, P. H., Baker, M. S., and Packer, N. H. (2009) Rat liver membrane glycoproteome: enrichment by phase partitioning and glycoprotein capture. *J. Proteome Res.* **8,** 770–781

40. Stavenhagen, K., Kolarich, D., and Wuhrer, M. (2015) Clinical glycomics employing graphitized carbon liquid chromatography-mass spectrometry. *Chromatographia* **78,** 307–320
41. Pabst, M., and Altmann, F. (2008) Influence of electrosorption, solvent, temperature, and ion polarity on the performance of LC-ESI-MS using graphitic carbon for acidic oligosaccharides. *Anal. Chem.* **80,** 7534–7542
42. Palmisano, G., Larsen, M. R., Packer, N. H., and Thaysen-Andersen, M. (2013) Structural analysis of glycoprotein sialylation -part II: LC-MS based detection. *Rsc. Advances* **3,** 22706–22726
43. Harvey, D. J. (1999) Matrix-assisted laser desorption/ionization mass spectrometry of carbohydrates. *Mass Spectrom. Rev.* **18,** 349–450
44. Harvey, D. J. (2005) Fragmentation of negative ions from carbohydrates: part 1. Use of nitrate and other anionic adducts for the production of negative ion electrospray spectra from N-linked carbohydrates. *J. Am. Soc. Mass Spectrom.* **16,** 622–630
45. Harvey, D. J. (2005) Fragmentation of negative ions from carbohydrates: part 2. Fragmentation of high-mannose N-linked glycans. *J. Am. Soc. Mass Spectrom.* **16,** 631–646
46. Harvey, D. J. (2005) Fragmentation of negative ions from carbohydrates: part 3. Fragmentation of hybrid and complex N-linked glycans. *J. Am. Soc. Mass Spectrom.* **16,** 647–659
47. Harvey, D. J., Jaeken, J., Butler, M., Armitage, A. J., Rudd, P. M., and Dwek, R. A. (2010) Fragmentation of negative ions from N-linked carbohydrates, part 4. Fragmentation of complex glycans lacking substitution on the 6-antenna. *J. Mass Spectrom.* **45,** 528–535
48. Harvey, D. J., and Rudd, P. M. (2011) Fragmentation of negative ions from N-linked carbohydrates. Part 5: Anionic N-linked glycans. *Int. J. Mass Spectrom.* **305,** 120–130
49. Harvey, D. J., Edgeworth, M., Krishna, B. A., Bonomelli, C., Allman, S. A., Crispin, M., and Scrivens, J. H. (2014) Fragmentation of negative ions from N-linked carbohydrates: part 6. Glycans containing one N-acetylglucosamine in the core. *Rapid Commun. Mass Spectrom.* **28,** 2008–2018
50. Harvey, D. J., and Abrahams, J. L. (2016) Fragmentation and ion mobility properties of negative ions from N-linked carbohydrates: Part 7. Reduced glycans. *Rapid Commun. Mass Spectrom.* **30,** 627–634
51. Harvey, D. J., Royle, L., Radcliffe, C. M., Rudd, P. M., and Dwek, R. A. (2008) Structural and quantitative analysis of N-linked glycans by matrix-assisted laser desorption ionization and negative ion nanospray mass spectrometry. *Anal. Biochem.* **376,** 44–60
52. Everest-Dass, A. V., Kolarich, D., Campbell, M. P., and Packer, N. H. (2013) Tandem mass spectra of glycan substructures enable the multistage mass spectrometric identification of determinants on oligosaccharides. *Rapid Commun. Mass Spectrom.* **27,** 931–939
53. Thomsson, K. A., Holmen-Larsson, J. M., Angstrom, J., Johansson, M. E., Xia, L., and Hansson, G. C. (2012) Detailed O-glycomics of the Muc2 mucin from colon of wild-type, core 1- and core 3-transferase-deficient mice highlights differences compared with human MUC2. *Glycobiology* **22,** 1128–1139
54. Schulz, B. L., Packer, N. H., and Karlsson, N. G. (2002) Small-scale analysis of O-linked oligosaccharides from glycoproteins and mucins separated by gel electrophoresis. *Anal. Chem.* **74,** 6088–6097
55. Schulz, B. L., Sloane, A. J., Robinson, L. J., Prasad, S. S., Lindner, R. A., Robinson, M., Bye, P. T., Nielson, D. W., Harry, J. L., Packer, N. H., and Karlsson, N. G. (2007) Glycosylation of sputum mucins is altered in cystic fibrosis patients. *Glycobiology* **17,** 698–712
56. Trombetta, E. S. (2003) The contribution of N-glycans and their processing in the endoplasmic reticulum to glycoprotein biosynthesis. *Glycobiology* **13**, 77r–91r
57. Varki, A.C. R., Esko, J. D., et al. editors. (2009) In: Essentials of Glycobiology. 2nd edition. Chapter 8 and Chapter 9. *Cold Spring Harbor (NY): Cold Spring Harbor Laboratory Press*
58. Varki, A., Cummings, R. D., Aebi, M., Packer, N. H., Seeberger, P. H., Esko, J. D., Stanley, P., Hart, G., Darvill, A., Kinoshita, T., Prestegard, J. J., Schnaar, R. L., Freeze, H. H., Marth, J. D., Bertozzi, C. R., Etzler, M. E., Frank, M., Vliegenthart, J. F., Lutteke, T., Perez, S., Bolton, E., Rudd, P., Paulson, J., Kanehisa, M., Toukach, P., Aoki-Kinoshita, K. F., Dell, A., Narimatsu, H., York, W., Taniguchi, N., and Kornfeld, S. (2015) Symbol nomenclature for graphical representations of glycans. *Glycobiology* **25,** 1323–1324
59. Ceroni, A., Maass, K., Geyer, H., Geyer, R., Dell, A., and Haslam, S. M. (2008) GlycoWorkbench: a tool for the computer-assisted annotation of mass spectra of glycans. *J. Proteome Res.* **7,** 1650–1659
60. Benjamini, Y., and Hochberg, Y. (1995) Controlling the false discovery rate: a practical and powerful approach to multiple testing. *J. Roy. Statistical Soc.* **57,** 289–300
61. Pinheiro, J., Bates, D., DebRoy, S., and Sarkar, D. (2012) (2013) R Development Core Team nlme: linear and nonlinear mixed effects models. R package version 3.1–103. *R Foundation for Statistical Computing, Vienna*
62. Tsuboi, S. (2012) Tumor defense systems using O-glycans. *Biol. Pharm. Bull.* **35,** 1633–1636
63. Suzuki, Y., Sutoh, M., Hatakeyama, S., Mori, K., Yamamoto, H., Koie, T., Saitoh, H., Yamaya, K., Funyu, T., Habuchi, T., Arai, Y., Fukuda, M., Ohyama, C., and Tsuboi, S. (2012) MUC1 carrying core 2 O-glycans functions as a molecular shield against NK cell attack, promoting bladder tumor metastasis. *Int. J. Oncol.* **40,** 1831–1838
64. Powers, T. W., Holst, S., Wuhrer, M., Mehta, A. S., and Drake, R. R. (2015) Two-dimensional N-glycan distribution mapping of hepatocellular carcinoma tissues by MALDI-imaging mass spectrometry. *Biomolecules* **5,** 2554–2572
65. Powers, T. W., Neely, B. A., Shao, Y., Tang, H., Troyer, D. A., Mehta, A. S., Haab, B. B., and Drake, R. R. (2014) MALDI imaging mass spectrometry profiling of N-glycans in formalin-fixed paraffin embedded clinical tissue blocks and tissue microarrays. *PLoS ONE* 9:e106255
66. Nie, H., Liu, X., Zhang, Y., Li, T., Zhan, C., Huo, W., He, A., Yao, Y., Jin, Y., Qu, Y., Sun, X. L., and Li, Y. (2015) Specific N-glycans of hepatocellular carcinoma cell surface and the abnormal increase of core-alpha-1, 6-fucosylated triantennary glycan via N-acetylglucosaminyltransferases-IVa regulation. *Sci. Rep.* **5,** 16007